Potential energy surfaces of ozone. I

Sotiris S. Xantheas, Gregory J. Atchity, Stephen T. Elbert, and Klaus Ruedenberg

Citation: J. Chem. Phys. **94**, 8054 (1991); doi: 10.1063/1.460140
View online: http://dx.doi.org/10.1063/1.460140
View Table of Contents: http://jcp.aip.org/resource/1/JCPSA6/v94/i12
Published by the American Institute of Physics.

Potential energy surfaces of ozone. I

Sotiris S. Xantheas,[a] Gregory J. Atchity, Stephen T. Elbert, and Klaus Ruedenberg
Ames Laboratory, United States Department of Energy and Department of Chemistry, Iowa State University, Ames, Iowa 50011

(Received 31 December 1990; accepted 11 March 1991)

The cross section through the ground-state potential energy surface of ozone which contains the open minimum, the ring minimum, and the ring-opening reaction path, including the ring-opening transition state, is determined through full-valence-space multiconfiguration self-consistent-field calculations. It is shown that, at a point on the ridge separating the open-structure basin from the ring-structure basin in C_{2v} symmetry, very close to the transition state, the ground-state surface connects with the lowest excited state surface of the same symmetry ($^1A_1$). This point is part of an intersection seam between these two $^1A'$ surfaces in C_s symmetry. It is furthermore found that the upper state has its equilibrium structure very close to the transition state of the lower state. The quantitative data of all critical points are calculated. In addition, a ground-state potential energy surface cross section describing the detachment of an oxygen atom is determined. For several other states, C_{2v} constrained and bond-length-optimized energy curves $E(\phi)$ are also reported.

I. INTRODUCTION

A. Experimental information

The relevance of ozone for life processes and, in particular, its presence in the upper atmosphere lends importance to experimental and theoretical studies of this molecule, its structure and spectra, its thermal reactions, and its photochemistry.

According to experimental evidence,[1] the ground state has a C_{2v} equilibrium structure with an apex angle of 116.8° and an O–O bond length of 1.278 Å. The molecule is a more potent oxidant than oxygen itself, a fact which can be related to the exothermicity of the reaction[2]

$$2O_3(\tilde{X}, {}^1A_1) \rightarrow 3O_2(X, {}^3\Sigma_g^-) + 69.5 \text{ kcal/mol}$$

at 0 K. This instability is surprising in view of the fact that two O_3 molecules contain four σ bonds and two delocalized three-center π bonds, whereas three O_2 molecules contain three σ bonds and three two-center π bonds. Combining the mentioned exothermicity with the spectroscopically known dissociation energy of oxygen[3]

$$O_2(\tilde{X}, {}^3\Sigma_g^-) \rightarrow 2O({}^3P) - 118.0 \text{ kcal/mol},$$

one obtains for the dissociation of O_3

$$O_3(\tilde{X}, {}^1A_1) \rightarrow O_2(X, {}^3\Sigma_g^-) + O({}^3P) - 24.2 \text{ kcal/mol}$$

at 0 K. This value is borne out by subtracting the ionization potential for $O_3 \rightarrow O_2^+ + O$ (302.7 kcal/mol) from that for $O_2 \rightarrow O_2^+$ (278.4 kcal/mol).[4,5] Since the vibrational zero-point energies are 2.26 kcal/mol and 4.09 kcal/mol for O_2 and O_3, respectively,[1,3] the energy differences between the equilibrium geometries exclusive of nuclear zero-point energies are found to be

$$E(2O) - E(O_2) = 120.3 \text{ kcal/mol},$$
$$E(2O_3) - E(3O_2) = 68.1 \text{ kcal/mol},$$
$$E(O_2 + O) - E(O_3) = 26.0 \text{ kcal/mol}.$$

The possible experimental error in the thermochemical reaction energy of $2O_3 \rightarrow 3O_2$ is quoted[2] as 0.8 kcal/mol.

The instability of ozone has caused early speculations regarding possible metastable species. Pulse radiolysis experiments of O_2 by Hochanadel, Ghormley, and Boyle[6] suggested the existence of a bound excited state which is stable to partial dissociation. Riley and Cahill[7] measured the half life of this species to be 5 μsec, but questioned whether it is in fact a vibrationally excited state as previously thought. Optical absorption measurements during pulse radiolysis of oxygen gas experiments by Bevan and Johnson[8] established the presence of two ozone precursors O_3^α and O_3^β, with absorption maxima at 315 and 285 nm, respectively, which they, too, attributed to vibrational excitations. Subsequently, Rosenberg and Trainor[9] identified the O_3^β species as being indeed vibrationally excited states, but Burton and Harvey[10] suggested that the O_3^α precursor, which shows absorption at 315 nm and has a lifetime of 5 μsec may correspond to a metastable species having D_{3h} symmetry.

B. Theoretical calculations

The last mentioned conjecture has its origin in the fact that *ab initio* calculations have established the existence of a second ground state minimum. It is a ring structure with D_{3h} symmetry which lies above the C_{2v} equilibrium structure in energy (only a two-configuration minimal-basis-set calculation yields the ring structure below the open structure).[11] The quantitative elevation of this ring minimum above the open minimum is still subject of debate. *Ab initio* calculations with double-zeta quality basis sets by Hay and Goddard[12] and by Hay, Dunning, and Goddard[13] yielded values of 27.6 kcal/mol and 34.5 kcal/mol, respectively, for this separation. Shih, Buenker, and Peyerimhoff[14] computed a value of 16 kcal/mol at the self-consistent-field configuration-interaction (SCF–CI) level. Hay, Dunning, and Goddard[15] obtained a value of 32.2 kcal/mol using generalized valence–bond (GVB)–CI wave functions, while Harding and Goddard[16] estimated the energy difference to be 27.3 kcal/mol in the GVB–POL–CI approximation. Using sing-

[a] Present address: Molecular Science Research Center, Pacific Northwest Laboratory, Washington 99352.

 0021-9606/91/128054-16$03.00

le + double excitation (SDCI) wave functions, Lucchese and Schaefer[17] predicted a value of 17.8 kcal/mol, whereas Hay and Dunning[18] gave a value of 28.0 kcal/mol in the generalized valence bond plus singles and doubles GVB + (1 + 2) level. Two-reference SDCI wave function calculations by Karlström, Engström, and Jönsson[19] based on multiconfiguration (MCSCF) orbitals yielded a value of 28.7 kcal/mol. Burton[20] used the paired-natural-orbital (PNO)–CI and coupled-electron-pair (CEPA) electron correlation methods with triple zeta plus polarization (TZP) basis set to calculate a value of 12.0 kcal/mol. Wilson and Hopper[21] report a value of 38.9 kcal/mol using a 76 configuration MCSCF/CI wave function which, however, predicts a ring state which is not of D_{3h} symmetry, but only approximately so. Density functional methods were used by Jones[22] who calculated the energy difference to be 32.3 kcal/mol. Recent studies by Moscardo, Andarias, and San-Fabian[23] (GVB calculations followed by CIPSI restricted configuration interaction) place the ring structure 21.1 kcal/mol above the ground state. The differences in the predicted separations between the minima are predominantly due to the differences in the configuration lists selected in the various investigations. This matter is discussed in some detail by the last mentioned authors.[23] Possibly the most accurate calculation of the minima to date is the very recent work by Lee[24] using the coupled cluster approach including single + double excitations and a perturbational estimate of triple excitations [CCSD(T)] based on a large [5*s*4*p*3*d* 2*f* 1*g*] atomic-natural-orbital (ANO) basis set and including the zero-point vibrational energy. This calculation yields a value of 28.7 kcal/mol for the separation between the minima and, hence, indicates that the ring minimum lies somewhat above the $O_2 + O$ dissociation limit.

Unresolved has remained the question how the surfaces on which the two minima lie are related to each other. Earlier SCF and GVB oriented investigations assigned them to different surfaces which were presumed to intersect somehow. Later investigators noted that the configurations characteristic of the two minima, being of the same symmetry, would combine to form two states of the same symmetry and these were presumed to avoid each other. The lower state would then contain the two minima and, at an intermediate geometry, a transition state. Interpolations of CI calculations in the intermediate region were made by Shih, Buenker, and Peyerimhoff,[14] by Karlström, Engström, and Jönsson,[19] and by Moscardo, Andarias, and San Fabrian[23] to estimate the transition state and these authors obtained ring opening barriers of 17.5,[14] 18.0,[19] 25.4,[19] and 19.13[23] kcal/mol, respectively. So far, no *ab initio* potential energy surface has been reported, however, which comprises both minima as well as the transition state. The only potential energy surfaces constructed for ozone to date are model surfaces.[25] Nor has the question been considered whether or how the two states, even though being of the same symmetry, might cross each other nonetheless.

C. Present investigation

In the present study, that part of the ground-state potential energy surface of ozone is determined which encompasses both minima, the transition state and the ring opening reaction path. An examination of this surface shows that there is, in fact, an element of truth in the earlier view which considers the two minima as belonging to different surfaces. This is because *a conical intersection seam is found to connect the ground-state surface with the excited state surface and to pass extremely close by the transition state.* This discovery of a conical intersection *between two states of the same symmetry in every applicable subgroup* in the ground state of a common molecule by accurate *ab initio* calculations is of interest because of the widespread skepticism regarding the actual occurrence of intersections between states of like symmetry. (Other work on conical intersections is discussed at the beginning of Sec. V.) In addition, we find that the excited state surface has its minimum in this very same region. This excited state equilibrium structure, the ring-opening transition state of the ground state, and the crossing of both surfaces all occur within 0.04 Å and 1 kcal/mol from each other. As regards the energy separation of the two minima, our results agree within 1 kcal/mol with those of Lee.[24]

We also report parts of the ground-state potential energy surface pertaining to the abstraction of the central atom and the detachment of an end atom to form $O_2 + O$.

A brief account of some of the present results was presented in a recent preliminary communication.[26]

II. METHOD

As mentioned above, the discrepancies between the quoted calculations are mostly due to differences in the configuration selection of the various MCSCF and CI wave functions. The reliable determination of potential energy surfaces requires a sufficiently flexible pool of configurations because different parts of the internal coordinate space can present very different bonding situations calling for a reshaping of the active orbitals as well as a redistribution of electrons among them. The important configurations from the various regions must be accounted for and sufficiently extended basis sets must be provided. However, the reliable determination of a potential energy surface requires energy calculations at many points. A compromise must therefore be struck so as to stay within the computational capabilities.

For the problem at hand, we consider an MCSCF calculation in the *full* configuration space generated by *all* valence orbitals (with the 1*s* orbitals remaining doubly occupied) a creditable, indeed a very appropriate compromise. It can be classified as a valence-space complete-active-space (CASSCF)[27] calculation. We have used this type of wave function under the name FORS (full optimized reaction space) wave function since 1976.[28] This approximation is chosen here. In O_3 there are 24 electrons and 15 molecular orbitals. The full configuration space is constructed by keeping the 1*s* orbitals of the three oxygen atoms doubly occupied and allowing the remaining 18 electrons to be distributed among the 12 active orbitals in all possible ways, thus creating the full valence space. The ground state belongs to the irreducible representations $^1A'$ and $^1A_1$ in the symmetry groups C_s and C_{2v}, respectively. For these irreps, the number of full-valence-space configurations is 8029 and 4067, respectively.

It is worth mentioning that coupled cluster and many-body perturbation methods based on single-reference wave functions, as used by Lee[24] for the very accurate determination of the minima, are not well suited for dealing with the problems addressed in the present investigation.

We have used a Dunning–Hay[29] basis set consisting of the segmented contractions $(9s5p1d/3s2p1d)$ yielding a total of 45 basis functions. For the d-type polarization function the exponent $\zeta_0 = 0.85$ was chosen.[29]

The geometry optimizing calculations of Sec. III were done with the program GAMESS of Dupuis *et al.*[30] The state-averaged MCSCF calculations in Sec. V were done with the program MOLPRO of Werner and Knowles.[31] Single-state calculations without geometry optimization in Secs. III and VI were done using both programs.

III. SINGLET STATES IN C_{2v} SYMMETRY WITH OPTIMIZED BOND LENGTHS

Initially, we examined the energies of the lowest $^1A_1$, $^1A_2$, $^1B_1$, and $^1B_2$ states as functions of the O–O–O angle ϕ, assuming isosceles triangle geometries, i.e., C_{2v} symmetry, with the bond length optimized. (The $^1A_2$, $^1B_1$, $^1B_2$ states have 3893, 3962, 3858 full-valence-space configurations, respectively, in C_{2v} symmetry.) The resulting energy curves are displayed in Fig. 1. The energy is plotted as a function of the apex angle ϕ for each value of which the O–O bond lengths are optimized. Several of these curves have more than one minimum. The internal coordinates of these minima are shown in Table I. The right end of the graph corresponds to the linear molecule. The left end corresponds to the abstraction of the center atom to infinity, while the two end atoms come together to form O_2.

As will be discussed in the next sections, the two ground-state minima at $\phi = 60°$ and 116.31° remain true minima upon asymmetric distortions when the symmetry is lowered to C_s. The lower minimum for an O–O–O angle of 116.31° and an O–O bond length of 1.299 Å corresponds to the experimentally observed equilibrium structure

TABLE I. Minima on the energy curves of Fig. 1.

State	$\phi°$	R(Å)	E (hartree)	ΔE[a] (kcal/mol)
$^1A_1$	116.31	1.299	−224.552 318	0.0
	60.00	1.470	−224.504 163	30.2
$^1A_2$	99.58	1.379	−224.496 017	35.2
$^1B_1$	111.92	1.482	−224.387 597	103.4
$^1B_2$	117.50	1.482	−224.478 977	46.0
	46.27	1.785	−224.407 440	90.9

[a] Relative to the ground-state minimum.

($\phi = 116.8°$, $R = 1.278$ Å). It lies 30.2 kcal/mol lower than the ring minimum on the $^1A_1$ ground-state potential energy surface (PES) which has equilateral geometry structure, i.e., D_{3h} symmetry with a bond length of 1.47 Å. Earlier comments[21] notwithstanding, the ring minimum connects to the dissociated products $O_2 + O$ in their ground states via abstraction (through a transition state) of the center atom.

For the other three states, $^1A_2$, $^1B_1$, and $^1B_2$, the Hessian matrices have a negative eigenvalue along the C_{2v} breaking normal mode at all minima shown in Fig. 1. These structures correspond therefore to *transition states* on the respective full potential energy surfaces in C_s.

IV. THE C_{2v} CONSTRAINED CROSS SECTION THROUGH THE GROUND-STATE POTENTIAL ENERGY SURFACE

A. The two minima

The wave function at the ring minimum and that at the open minimum differ in their dominant Hartree–Fock SCF determinants. Both of these consist of doubly occupied orbitals only, corresponding to a $\sigma^{12}\pi^6$ structure for the former and a $\sigma^{14}\pi^4$ structure for the latter in the valence space. These two valence configurations are illustrated in Fig. 2. In addition to the inner shells, they agree in the occupations of 14 electrons: one sigma lone pair for each of the three atoms, one bond pair for each of the sigma bonds along the two legs

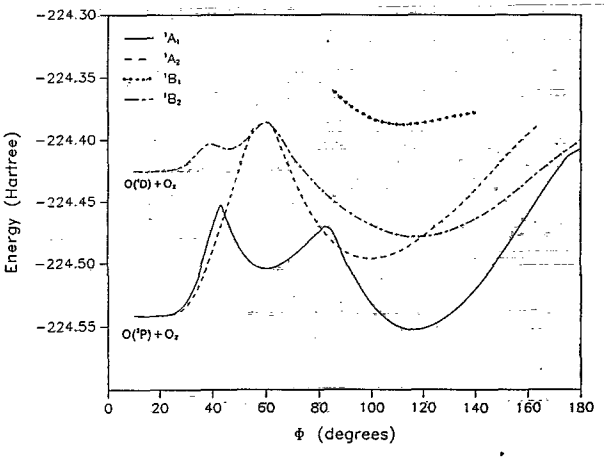

FIG. 1. Energies of the lowest $^1A_1$, $^1A_2$, $^1B_1$, and $^1B_2$ states of O_3 in C_{2v} symmetry as a function of the O–O–O angle ϕ with the O–O distances optimized for each ϕ. In the dissociation products for $\phi \to 0$ (abstraction of the center atom), the O_2 molecule is in its ground state ($X\,^3\Sigma_g^-$) for both limits shown.

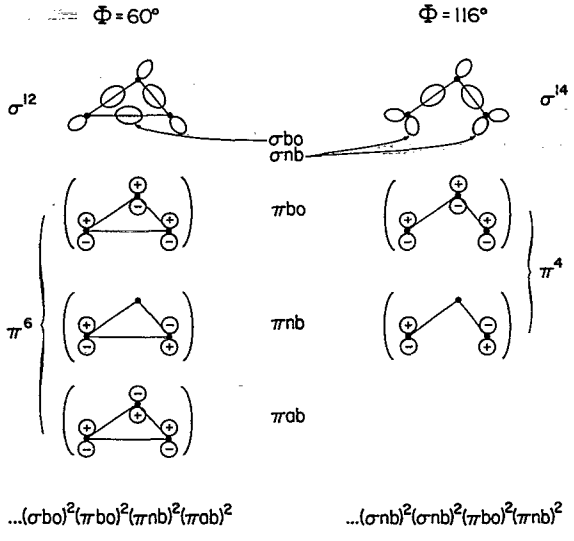

FIG. 2. Dominant configurations for the two minima on the PES of the $^1A_1$ ground state of O_3.

TABLE II. Harmonic frequencies (in cm^{-1}) for the two minima on the ground-state potential energy surface of ozone.

	This work	Lee[a]	Experiment[b]
	Ring minimum (D_{3h})		
$\nu_1(e')$	750	795	
$\nu_2(a_1')$	1046	1114	
	Open minimum (C_{2v})		
ν_1	685	718	705
ν_2	1044	1053	1042
ν_3	1093	1153	1110

[a] Reference 24.
[b] Reference 1, p. 604.

of the isosceles triangle, one pair in a π bonding orbital, another in a π nonbonding orbital. The remaining four electrons are distributed among the sigma bonding and antibonding orbitals between the end oxygens and the π-antibonding orbital. In the ring structure, the sigma bonding and the π-antibonding orbitals are occupied. In the open structure, the π-antibonding orbital is empty and the sigma bonding and antibonding orbitals are both occupied, effectively forming two sigma nonbonding lone pairs, one on each end atom. The valence orbital occupations can thus be expressed as follows. Open structure minimum: dominant valence configuration $=\sigma^{12}(\sigma^*)^2\pi^4$; ring structure minimum: dominant valence configuration $=\sigma^{12}\pi^4(\pi^*)^2$. The complete sets of dominant symmetry orbital occupations are $(1a_1)^2(1b_1)^2(2a_1)^2(3a_1)^2(4a_1)^2(2b_1)^2(5a_1)^2(3b_1)^2(6a_1)^2(4b_1)^2(1b_2)^2(1a_2)^2$ for the open structure and $(1a_1)^2(1b_1)^2(2a_1)^2(3a_1)^2(4a_1)^2(2b_1)^2(5a_1)^2(3b_1)^2(6a_1)^2(1b_2)^2(1a_2)^2(2b_2)^2$ for the ring structure, with the conventional assumptions about the axes (y axis perpendicular to the molecular plane, z axis bisecting the apex angle). It is apparent that both configurations belong to the irreducible representation $^1A_1$ and hence, this is also the case for the full wave functions at the two minima. It should be noted that from Sec. IV B on, we shall display C_{2v} constrained potential energy plots in terms of internal coordinates X, Y which are related to the just mentioned axis coordinates by $X=x$, $Y=z$.

The geometries of both, the open minimum and the ring minimum, were determined by unconstrained minimizations in C_s symmetry. For the ring minimum this resulted in perfect D_{3h} symmetry. For the open minimum, it resulted in perfect C_{2v} symmetry. The data are included in Table I. We also determined the Hessian and the normal vibrational mode frequencies for both minima. For the ring minimum, two frequencies are degenerate, belonging to the irrep E', the third to the irrep A'. The values of all frequencies are listed in Table II, together with those obtained by Lee[24] and the experimental values listed by Herzberg[1] for the open structure. Considering that our wave function is considerably simpler than Lee's, the agreement is gratifying.

These theoretical harmonic frequencies yield values of 4.03 and 3.63 kcal/mol for the zero-point vibrational energy at the open and ring minimum, respectively. Including these corrections, the energy separation between the two minima becomes 29.8 kcal/mol which differs by about 1 kcal/mol of Lee's[24] value of 28.7 kcal/mol. It is therefore most likely that the ring minimum lies slightly above the experimental O_2+O dissociation limit which, as noted before, is 24.2 kcal/mol above the ground state. This ordering would contribute to the difficulty of accessing the ring structure by direct excitation from the lower open structure.

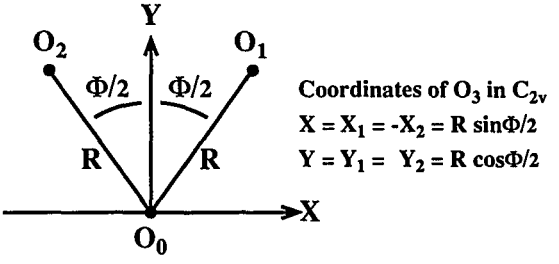

FIG. 3. C_{2v} constrained coordinates.

B. The C_{2v} constrained potential energy surface

We shall display the C_{2v} ($R_1=R_2=R$) constrained potential energy surfaces (PES') with respect to coordinates X, Y whose definition and meaning are illustrated in Fig. 3: If one places the center atom at the origin $X=Y=0$, then (X,Y) are simply the coordinates of one of the end atoms and $(-X,Y)$ are the coordinates of the other end atom.

Figure 4 exhibits the contours $E(\phi,R)$ for the C_{2v} constrained cross section through the ground-state PES. The

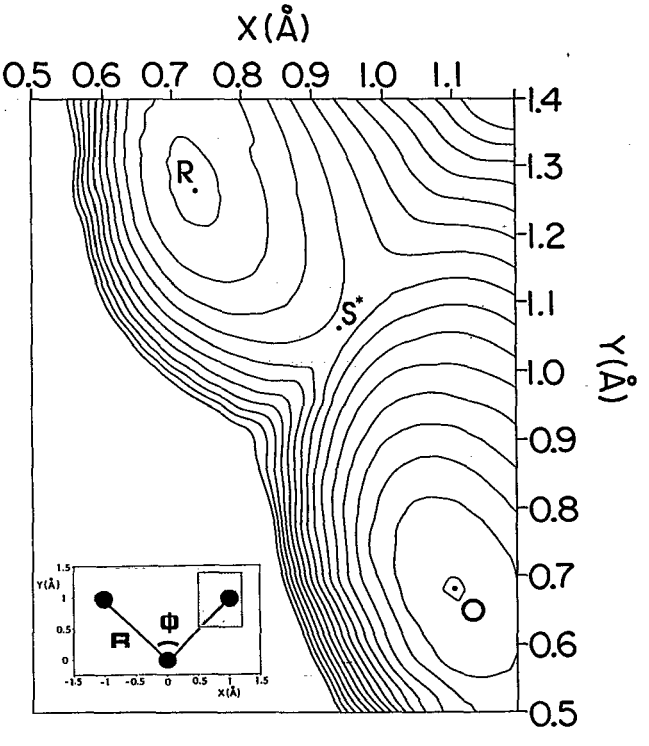

FIG. 4. C_{2v} constrained PES of the $^1A_1$ ground state of ozone pertinent to the opening of the D_{3h} ring. Increment: 10 millihartree. R: ring minimum, O: open minimum, S^*: saddlepoint. Contours based on 130 evenly spaced calculated values. Single-state calculations.

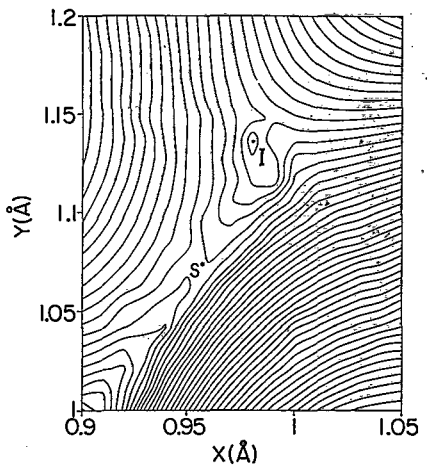

FIG. 5. Ground state C_{2v} constrained PES near the ring opening transition state. S^*: saddle point, I: intersection point. Increment: 0.1 millihartree. Contours based on 40 evenly spaced calculated values. Single-state calculations.

inset in Fig. 4 illustrates the range covered by the displayed portion of the PES. The contours correspond to energy increments of 10 millihartree (6 kcal/mol). They are derived from a set of 130 calculated points which are evenly distributed over the plotted area. The ring minimum is denoted by R, the open minimum is denoted by O. The surface is clearly divided into a ring structure basin, an open structure basin, and a ridge between them.

The lowest point on the ridge which separates the ring from the open structure basin, denoted by S^*, is a saddle point. An enlarged view of the region around S^* is provided by Fig. 5, where the contours are drawn at energy increments of 0.1 millihartree (0.06 kcal/mol). This plot is based on 40 evenly distributed calculated energy values. The contours near the point denoted by I are not spurious but, as we shall see, are due to an intersection of this surface with an excited state surface. The latter has the following origin.

As can be seen from Fig. 5, the slope down from the ridge is much steeper on the open-structure-basin side (lower right) than on the ring-structure-basin side (upper left). This difference is due to the fact that the dominant part of the ground-state wave function is different in the two regions, as discussed in detail in Sec. IV A and that the wave function rapidly exchanges its dominant configurations when one passes across the ridge. In such a situation, there exists an excited state of the system whose wave function exhibits the converse behavior. On the left side of the ridge, its dominant configurations are those which dominate the ground state on the right side of the ridge and vice versa. Both states are superpositions of the same configurations and, hence, have the same symmetry, namely $^1A_1$. Usually, the energies of two such states come close upon approach to the region of the ground-state ridge and then "repel" each other. As a result, the energy of the excited state has a valley where the ground state has a ridge. However, in the case at hand, the situation is different: We shall show, in Sec. V, that the two states *touch each other in a point* near I in the C_{2v} constrained coordinate space. The two states furthermore *intersect each other along a line* in the full coordinate space (C_s symmetry). Instead of an "avoided crossing," we have here a "conical intersection seam" between two states of like symmetry.

C. Transition state and ring opening

Because of the closeness of the two surfaces near their intersection point, numerical difficulties were encountered for the ground-state MCSCF calculation in the close neighborhood of S^* and I and, hence, in finding the exact position of the saddle point. This was because the single-state CI eigenvalue procedure used seeks the eigenvector closest to the initial guess which, in these calculations was taken from a nearby geometry. Upon passing the ridge, the eigenvector of the ground state becomes however a close approximation to the eigenvector of the higher state when the energy gap is very small. [See Sec. V A(iv) below regarding this property of surface crossings.] It was, in fact, this slippage between the two surfaces which alerted us to the possibility of an intersection.

In order to overcome this problem and, also, to locate the intersection point, we first determined both surfaces in this region by means of *state averaged* MCSCF calculations in the full valence space, with both states being given equal weight. (All previously discussed results, including the plots in Figs. 4 and 5, were obtained by single-state MCSCF calculations in the full valence space). The coordinates (ϕ^*, R^*) of S^* were determined as the saddle point of a quadratic polynomial in ϕ and R which was least-mean-squares fitted, with a relative mean deviation of 1.4%, to 50 points in the domain defined by

$$83.3^\circ \leqslant \phi \leqslant 83.8^\circ, \quad 1.42 \text{ Å} \leqslant R \leqslant 1.46 \text{ Å}.$$

The coordinates of S^* were found to be $\phi^* = 83.574^\circ$, $R^* = 1.438$ Å.

The question whether this point is the transition state for the ring opening was settled by calculating the energy for the C_{2v} symmetry breaking displacement with the coordinates $\phi = \phi^* = 83.574^\circ$, $R_1 = R^* + 0.01$ Å $= 1.448$ Å, $R_2 = R^* - 0.01$ Å $= 1.428$ Å. The energy at this point was found to lie 73 microhartree above that at S^* showing that the C_{2v} symmetry-breaking mode has a positive eigenvalue of the Hessian. The other two eigenvalues of the Hessian are C_{2v} symmetry preserving and it is evident from Figs. 4 and 5 that one of them is positive and the other is negative. The point S^* is therefore the transition state for the ring opening.

The eigenvectors and eigenvalues of the Hessian in C_{2v} at the transition state were found to be

$$\mathbf{t}_\parallel = (0.562\,079, 0.827\,084), \quad \lambda_\parallel = 0.852\,787 \text{ hartree/Å}^2,$$
$$\mathbf{t}_\perp = (-0.827\,084, 0.562\,079),$$
$$\lambda_\perp = -230.669 \text{ hartree/Å}^2,$$

where $\mathbf{t}_\parallel$ and $\mathbf{t}_\perp$ are expressed in terms of the coordinates (X, Y) defined in Sec. IV B. It is apparent from the eigenvalues that $\mathbf{t}_\parallel$ points along the ridge of the barrier separating the two basins and $\mathbf{t}_\perp$ points in the direction of the reaction path. It is also readily seen that $\mathbf{t}_\parallel$ forms an angle of 7.59° with the vector point from the origin to the transition state position S^*, viz.,

$$\mathbf{R}^* = (X^*, Y^*) = R^*(\sin\phi^*/2, \cos\phi^*/2)$$
$$= R^*(0.666\,352, 0.745\,637).$$

TABLE III. Geometries and energies of critical points.[a,b]

	$1\,^1A_1$ Open minimum		$1\,^1A_1$ Ring minimum	
	S–S Determined	S–A Determined	S–S Determined	S–A Determined
R(Å)	1.298	1.305	1.470	1.476
ϕ(degree)	116.32	116.04	60.00	59.97
E_1(S–S calculation)	− 224.552 317	− 224.552 251	− 224.504 163	− 224.504 126
E_1(S–A calculation)	− 224.545 111	− 224.545 195	− 224.497 800	− 224.497 832
E_1(S–A calculation) − E_1(S–S calculation)	0.007 206	0.007 056	0.006 363	0.006 294
E_2(S–A calculation)	− 224.397 013	− 224.400 152	− 224.214 214	− 224.218 451
E_2(S–A calculation) − E_1(S–A calculation)	0.148 098	0.145 043	0.283 586	0.279 381

	$2\,^1A_1$ Minimum	$1\,^1A_1$ Transition state		Intersection
	S–A Determined	S–S Determined	S–A Determined	S–A Determined
R(Å)	1.441	1.431	1.438	1.476
ϕ(degree)	83.59	83.86	83.57	83.18
E_1(S–S calculation)	···	− 224.467 986	− 224.468 315	− 224.466 664
E_1(S–A calculation)	− 224.463 474	− 224.464 249	− 224.463 393	− 224.462 188
E_1(S–A calculation) − E_1(S–S calculation)	···	0.003 737	0.004 922	0.004 476
E_2(S–A calculation)	− 224.463 164	− 224.462 893	− 224.463 037	− 224.462 180
E_2(S–A calculation) − E_1(S–A calculation)	0.000 31	0.001 356	0.000 356	0.000 008

[a] All energies in hartree.
[b] S–S = single-state calculation, S–A = state-averaged calculation.

Since this vector is, in fact, the vector from the central oxygen to the terminal oxygen, it follows that, at the transition state, the deformation of the molecule along the reaction path corresponds to a motion of the terminal oxygen which is, within about 7° degrees, perpendicular to the direction of its bond to the central oxygen, i.e., it is almost a pure bending motion. The magnitude of the force constant along the ridge, $k_{\|} = 2\lambda_{\|}$, is of the order of magnitude found in diatomic molecules [e.g., $k(\mathrm{HF}) \approx 2$ hartree/Å^2]. The large magnitude of $\lambda_{\perp}$ shows that the barrier is extremely steep along the reaction coordinate. This is because the switchover between the dominant configurations discussed in Sec. IV A occurs very fast along this coordinate.

Starting with the wave functions from the state-averaged calculation, we determined the transition state for the single-state FORS calculation at $\phi^* = 83.86°$, $R^* = 1.431$ Å. Conversely, the ring minimum and the open minimum were also determined with state-averaged calculations.

The quantitative results for the discussed calculations of the transition state and the two minima (as well as for other calculations to be discussed further on) are listed in Table III. In it, the energies collected *in one column* are the results of various calculations *at one geometry*, namely the R and Φ values given in the first two rows. The determinations of these geometries are characterized by the descriptive column heads. The energy deviations between the two types of calculations at any one point vary from 2 to about 4 kcal/mol. The resulting energy differences between the critical points are listed in Table IV. The *corresponding* differences [i.e., single-state (SS) energies at SS determined geometries and state-averaged (SA) energies at SA determined geometries] vary only between 0.2 and 1.6 kcal/mol. In view of the fact that both states are being given equal weight in the state averaging, these deviations are gratifyingly small. The ring opening barrier is seen to be 22.7 kcal/mol. The ring closing barrier, on the other hand, is 52.9 kcal/mol which is more than twice the energy for detaching an oxygen atom from ozone in its ground state (see Sec. I A).

It follows from general symmetry considerations that

TABLE IV. Energy differences between critical points (kcal/mol). Zero-point vibrational energy differences are not included. They are discussed in Sec. IV A.

Molecular geometries between which differences are calculated	Energies obtained from: Single-state calculation	Energies obtained from: State-averaged calculation
Ring minimum minus open minimum		
Single-state optimized geometries	30.2	29.7
State-averaged optimized geometries	30.2	29.7
Transition state minus open minimum		
Single-state optimized geometries	52.9	50.7
State-averaged optimized geometries	52.7	51.3
Transition state minus ring minimum		
Single-state optimized geometries	22.7	21.1
State-averaged optimized geometries	22.5	21.6
Intersection minus transition state		
State-averaged optimized geometries	1.0	0.8

the steepest descent line which begins at S^* along the reactive mode with the negative Hessian eigenvalue will preserve C_{2v} symmetry until it reaches a minimum. Thus, the entire ring opening reaction proceeds along a path which maintains C_{2v} symmetry throughout. As a confirmation, we also examined the C_{2v} symmetry breaking distortions for several points on the $^1A_1$ curve in Fig. 1 [$E(\phi)$ optimized with respect to $R_1 = R_2 = R$]. For $\phi = 65°$, 70°, 80°, 85°, 90°, 95°, 100°, and 110° we calculated the energy for $R_1 = R(\phi) + 0.01$ Å, $R_2 = R(\phi) - 0.01$ Å, where $R(\phi)$ is the C_{2v} optimized value of R for ϕ. In all cases, the energy increased implying that this path lies in fact at the bottom of a C_{2v} preserving valley.

V. THE INTERSECTION BETWEEN THE GROUND STATE AND THE LOWEST EXCITED STATE OF LIKE SYMMETRY

The only past *ab initio* evidence for a crossing between two states belonging to the same irreducible representation *in every applicable symmetry group* has been the inference from the wave function phase change (see below) in a calculation[32] of LiNaK modeled after H_3 (where the intersection occurs at a point of D_{3h} symmetry) and a Frost-model calculation[33] of CH_4^+ near a point of high symmetry. Very recently, since the completion of the present investigation, an *ab initio* surface crossing seam between two states of like symmetry has also been reported as exceedingly likely ($E_2 - E_1 < 0.64\,\mu$h) for the system H_2 + He by Manaa and Yarkony.[34] In no other molecule has such an intersection as yet been found by accurate *ab initio* calculation and skepticism regarding the physical relevance of crossings between states of like symmetry has remained widespread. It is therefore essential to carefully document the claim that such a crossing does indeed occur on the ground-state surface of ozone. The relevant criteria emerge from certain fundamental properties of surface intersections which are summarized below.

A. Theoretical characteristics of an intersection between two PES'

The formal analysis of conical intersections goes back to papers by Hund, von Neumann and Wigner,[35] Teller,[36] Herzberg and Longuet-Higgins[37] and has continued into recent times.[38–40] A brief discussion of the elementary relations and details relevant here is also given in a recent paper by the present authors.[41] In the present context, the following facts are pertinent.

(i) When two states belonging to the same irreducible representation intersect, then they do so in a curvilinear coordinate space of dimension $(Q-2)$, where Q is the total number of internal coordinates. In a triatomic molecule, the full internal coordinate space is of dimension 3 and the intersection space is of dimension $3 - 2 = 1$, i.e., a line called the intersection seam. The C_{2v} constrained coordinate subspace is of dimension 2 and the intersection space is of dimension $2 - 2 = 0$, i.e., an intersection point. It is the point where the intersection seam traverses the C_{2v} subspace at right angles.[35,36]

(ii) If one defines displacements (ξ,η) from a point (x_c,y_c) on the intersection seam, in a plane perpendicular to the seam at (x_c,y_c), then the energy difference between the two states in the immediate neighborhood of (x_c,y_c) is given by an elliptical cone, viz.,

$$E_2 - E_1 = (a\xi^2 + b\eta^2 + 2c\xi\eta)^{1/2},$$

whereas the average of the two energies is given by a plane

$$(E_1 + E_2)/2 = A\xi + B\eta.$$

This is true in particular around the intersection point in the C_{2v} constrained plane.[36]

(iii) If one follows the continuous deformations of any one of the two state wave functions along a *closed* path looping around the intersection point (x_c,y_c) in the two-dimensional plane perpendicular to the seam, then the wave function will return to its original form *multiplied by* (-1), provided this is the only intersection inside the loop. If the loop contains no intersection, the wave function returns to its original value.[37]

(iv) If one moves through the intersection along any straight line in the just-mentioned plane, then the wave function of the lower surface will become identical to that of the higher surface (aside from a possible phase factor) at the intersection, and vice versa.[41] This relationship between the wave functions can create numerical problems as mentioned in the beginning of Sec. IV C.

B. Determination of the intersection point in C_{2v}

In order to find the intersection, we must calculate energies for the two states of the same symmetry. As mentioned earlier, this was accomplished by two-state-averaged MCSCF calculations in the full valence space using the same basis set as before. Both states were given equal weight. Because of the state averaging, the energies obtained for the ground state are of course slightly higher than the single-state MCSCF results as was already noted earlier (Tables III and IV).

1. Passes across the ridge

According to the dimensionality rules explained under (i) in Sec. V A, the two surfaces intersect only at isolated points in the (R,ϕ) plane and these are not distinguished by any other characteristics. To home in on the region where the conjectured intersection might occur, we determined the energies of both states along several passes across the ridge of Fig. 5. Since, as discussed in Sec. IV C, the ridge is approximately a line ϕ = constant, calculations were made for the following points:

R(Å)	Range of ϕ	$\Delta\phi$	No. of of points
1.42	83.74° to 83.82°	0.01°	9
1.43	83.63° to 83.72°	0.01°	10
1.44	83.54° to 83.63°	0.01°	10
1.45	83.42° to 83.52°	0.01°	11
1.46	83.32° to 83.40°	0.01°	9
1.47	83.20° to 83.28°	0.01°	9
1.48	83.10° to 83.18°	0.01°	9
1.49	82.99° to 83.06°	0.01°	8

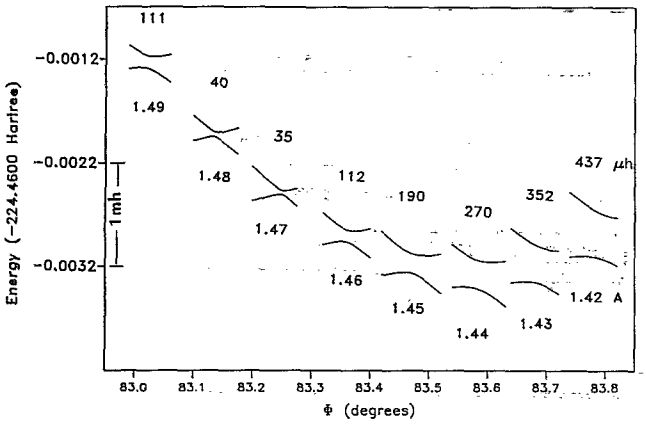

FIG. 6. Energies of the two lowest $^1A_1$ surfaces on various passes across the ground-state PES ridge of O_3 near the transition state. The energy separation of the two states is indicated above the curves in microhartree. Each set of curves corresponds to a different R value which is indicated (in Å) below them. State-averaged calculations.

The points for a given R value yield one pass across the ridge. The energies of the two states are displayed, for each pass, in Fig. 6 above the R value identifying that pass. The figure collects eight separate graphs.

For each pass, the lower energy shows a maximum and thus moves across the ridge whereas the upper energy has a minimum and thus traverses a valley. The minimum of the maxima on the lower energy curves is the earlier determined transition state S^*. The numbers listed in Fig. 6 *above* each upper state curve are the energy splits (in microhartree) between the maximum of the energy curve of the lower state and the minimum of the energy curve of the upper state. It is apparent that this gap goes through a minimum of less than 35 microhartree between $R = 1.47$ Å and $R = 1.48$ Å, with ϕ lying between 83.1° and 83.3°. The intersection, if it exists, must therefore lie in this region.

2. Difference cone

Having narrowed down the location of the intersection, we calculated energies of the two states for additional points in the identified region. If an intersection exists, then, as discussed under (ii) in Sec. V A *the energy difference* $(E_2 - E_1)$ *must vary as the square root of a quadratic form in terms of the displacements from the intersection*. Accordingly, we proceeded to approximate the quantity $(E_2 - E_1)^2$ by a quadratic polynomial ΔE^2 in terms of $\xi = (X - X^*)$ and $\eta = (Y - Y^*)$, the displacements from the transition state S^* expressed in terms of the coordinates defined in Sec. IV B. The fit of ΔE^2 to $(E_2 - E_1)^2$ was accomplished by a least-mean-squares calculation based on 19 points in the range $83.11° \leqslant \phi \leqslant 83.27°$, 1.47 Å $\leqslant R \leqslant$ 1.48 Å and resulted in an approximation ΔE to $(E_2 - E_1)$ with a mean absolute deviation of 2.5 microhartree. Since the minimum of this quadratic fit ΔE^2 should yield an approximation to the intersection point I, it is expected to be zero. However, it turned out slightly negative [$-$ (18 microhartree)^2]. We therefore incorporated the condition that ΔE^2 should vanish at its minimum by iterating the least-mean-squares (LMSQ) procedure after including, as a twentieth point, the value $(E_2 - E_1) = 0$, with a weight factor of 200, at the position of the minimum found in each preceding iteration. In this manner, the minimum value of ΔE^2 could be raised to [$-$ (2 microhartree)^2] without increasing the mean absolute deviation (2.5 microhartree) of ΔE from $(E_2 - E_1)$. All relevant quantitative data of this final fit are listed in Table V. (The values in it differ somewhat from those reported in Ref. 26 because of the difference in the coordinates and the attempt to annihilate ΔE at the minimum.) Its high quality should be contrasted with the *unsatisfactory result of an attempt to fit* $(E_2 - E_1)$ *directly with a quadratic*: The latter was not only found to have a mean absolute deviation of 11 microhartree, but, furthermore, had one *negative* eigenvalue.

Taking the minimum of the fit documented in Table V as the intersection point, one finds for the vector **d**, pointing from the transition state S^* to the intersection I, the X,Y coordinates

$$S^* \rightarrow I = \mathbf{d} = (0.021\,330, 0.031\,389)\ \text{Å}.$$

Thus, *these two points lie only* 0.038 Å *apart*. The vector **d** forms an angle of 7.56° with the bond vector **R*** introduced in Sec. IV C and an angle of 0.029° with the normal mode vector $\mathbf{t}_\parallel$, also found in Sec. IV C, which points along the barrier ridge at the transition state. The intersection point thus lies essentially *on* the barrier ridge very close to the

TABLE V. Fit of energy difference between the lowest two $^1A_1$ state of ozone near the conical intersection (in μh).[a]

ϕ(deg)	R(Å)	ξ[b]	η[b]	E_2–E_1(μh)	ΔE = LMSQ Fit[c] (μh)
83.200	1.4700	0.017 682	0.026 985	332	331
83.240	1.4700	0.018 066	0.026 644	73	80
83.250	1.4700	0.018 161	0.026 559	35	44
83.260	1.4700	0.018 257	0.026 474	77	78
83.270	1.4700	0.018 353	0.026 389	140	136
83.175	1.4725	0.019 101	0.029 067	306	305
83.200	1.4725	0.019 342	0.028 854	142	143
83.250	1.4725	0.019 822	0.028 427	190	188
83.150	1.4750	0.020 520	0.031 151	281	281
83.175	1.4750	0.020 761	0.030 937	117	117
83.225	1.4750	0.021 242	0.030 510	210	211
83.125	1.4775	0.021 938	0.033 235	257	259
83.150	1.4775	0.022 179	0.033 021	96	95
83.200	1.4775	0.022 661	0.032 593	232	234
83.110	1.4800	0.023 452	0.035 234	171	173
83.130	1.4800	0.023 645	0.035 063	54	49
83.140	1.4800	0.023 742	0.034 977	47	41
83.150	1.4800	0.023 838	0.034 892	99	98
83.160	1.4800	0.023 935	0.034 806	161	161
83.185	1.4757	0.021 330	0.031 390	8	1*i*

[a] μh = microhartree/molecule $\simeq$ 0.6 cal/mol.

[b] $\xi = X - X^*$, $\eta = Y - Y^*$, with (X^*, Y^*) = transition state coordinates.

[c] Fit: $\Delta E = \{0.185\,557\,531\ \xi^2 + 0.079\,626\,935\ \eta^2 - 0.242\,988\,733\ \xi\eta - 0.000\,288\,338\,38\ \xi + 0.000\,183\,859\,97\ \eta - 1.89\,800 \times 10^{-7}\}^{1/2}$. Mean absolute deviation = 2.44 μh = 0.82% of $(E_2 - E_1)$ range. Minimum: $\xi = 0.021\,438\,1$ Å, $\eta = 0.031\,555\,6$ Å, $\Delta E_{\text{Min}} = 2.06i$ μh. Eigenvectors (X,Y components) and eigenvalues of ΔE^2 at intersection: $c_\parallel = (0.547\,894,\ 0.836\,548)$, $\lambda_\parallel = 0.000\,054\,676\,6$ hartree^2/Å^2, $c_\perp = (0.836\,548, -0.547\,894)$, $\lambda_\perp = 0.265\,130$ hartree^2/Å^2, where $c_\parallel$ lies along the barrier ridge and $c_\perp$ perpendicular to it. The fit ΔE^2 is negative for points with projections along $c_\parallel$ and $c_\perp$ being less than 3×10^{-4} Å and 4×10^{-6} Å, respectively.

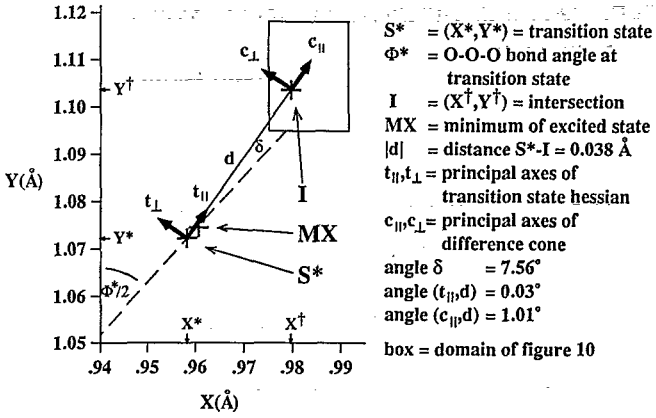

FIG. 7. Locations of the ground-state transition state, the excited state minimum, and the intersection of both states in coordinate space. The dotted line is along the O_0O_1 bond.

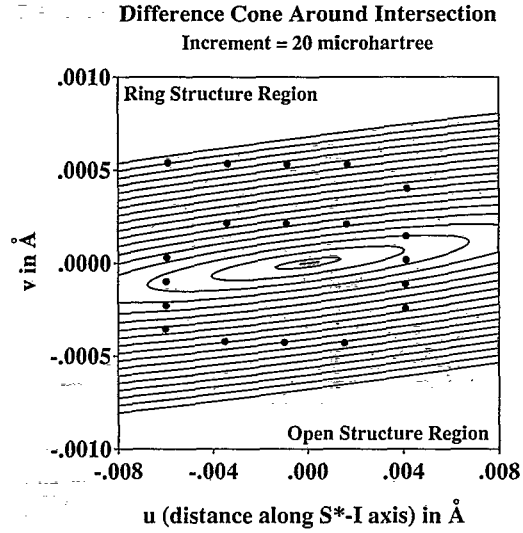

FIG. 9. Contours of the square root of the quadratic fit to the squares of the energy differences of the two lowest $^1A_1$ states of ozone around their intersection at the 19 points (in C_{2v} symmetry) indicated by heavy dots.

transition state. The geometrical relations between the direction of the bond vector $O_0 \rightarrow O_1 = \mathbf{R}^*$, the vector $S^* \rightarrow I = \mathbf{d}$, and the normal mode vectors $\mathbf{t}_\parallel$, $\mathbf{t}_\perp$ are illustrated in Fig. 7. Also shown in that figure are the principal axes vectors $\mathbf{c}_\parallel$ and $\mathbf{c}_\perp$ of the quadratic fit ΔE^2. The components of $\mathbf{c}_\parallel$ and $\mathbf{c}_\perp$ are listed in Table V and it is seen that $\mathbf{c}_\parallel$ forms an angle of 8.56°, with the bond vector $\mathbf{R}^*$ and an angle of 1.006° with the vector $\mathbf{d} = S^* \rightarrow I$. Therefore it too lies essentially along the barrier ridge. The relation of Fig. 7 to the earlier global potential energy surfaces is provided by Fig. 8 which exhibits the relative sizes and locations of the domains covered in Figs. 4, 5, and 7, respectively. (Fig. 7, in turn, contains an inset of a still smaller domain which will be examined below in Fig. 10.)

Since both the Hessian at the transition state as well as the quadratic fit ΔE^2 at the intersection point have one eigenvector very nearly parallel to the vector $\mathbf{d}$ connecting the transition state and the intersection, it is practical to use the projections onto the unit vectors parallel and perpendicular to $\mathbf{d}$, viz.,

$$\mathbf{e}_\parallel = (0.562\,047,\ 0.827\,105)\ \text{Å},$$

$$\mathbf{e}_\perp = (-0.827\,105,\ 0.562\,047)\ \text{Å},$$

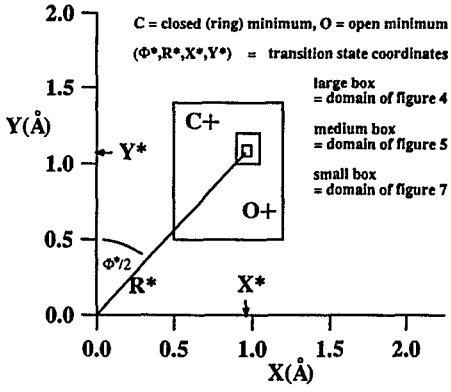

FIG. 8. Relative locations of various examined domains in coordinate space.

as coordinates. We shall call them u and v, respectively. The intersection point is chosen as the origin.

These coordinates are used in Fig. 9 to display a contour plot of the square root approximation ΔE, documented in Table V. Since the two eigenvalues listed in that table are seen to differ from each other by three to four orders of magnitude, a different scale is used for u and v in the drawing. The plot exhibits the equidistant contours typical for a cone. The contour increment is 20 microhartree. The short straight line in the center (actually a very narrow ellipse) is the contour $\Delta E = 0$. It is "inside" this contour that ΔE^2 is negative as mentioned above. The 19 points on which the fit is based are also shown. In terms of Fig. 7, the domain of Fig. 9 is centered around I with the u axis parallel $\mathbf{d}$, the range of u being slightly longer than one of the fat arrows, the range of v about as wide as an arrow tip at its widest point.

A calculation of E_1 and E_2 at the presumed intersection point yielded the actual energy difference $E_2 - E_1 = 7.6$ microhartree (see Tables III and V). There would be no difficulty in searching for further points where the energy differences between the two states are even smaller. However, the question whether there really exists a true intersection in the C_{2v} subspace would not thereby be settled. There is only one definitive way to resolve this question, namely to examine the phase of the wave function: According to criterion (iii) discussed in Sec. V A, the wave function changes sign when followed continuously on a closed path looping around an intersection point. Such calculations seemed therefore more useful.

3. Phase change of the wave function

How can we monitor the sign of the wave function? In the neighborhood of the saddle point, the ground-state wave function has four dominant configurations and all four consist of doubly occupied orbitals only. Consequently, the signs of these configurations are unaffected by any changes in *orbital* phases and the sign of the total wave function is

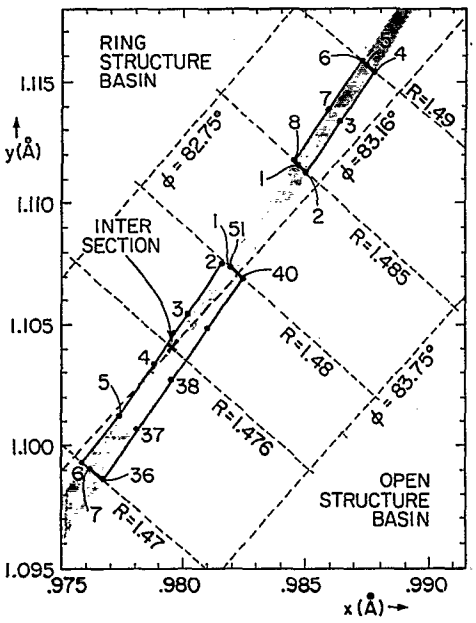

FIG. 10. Two loops crossing the ground-state ridge: one enclosing the intersection, the other not enclosing the intersection. The shaded region indicates the ridge.

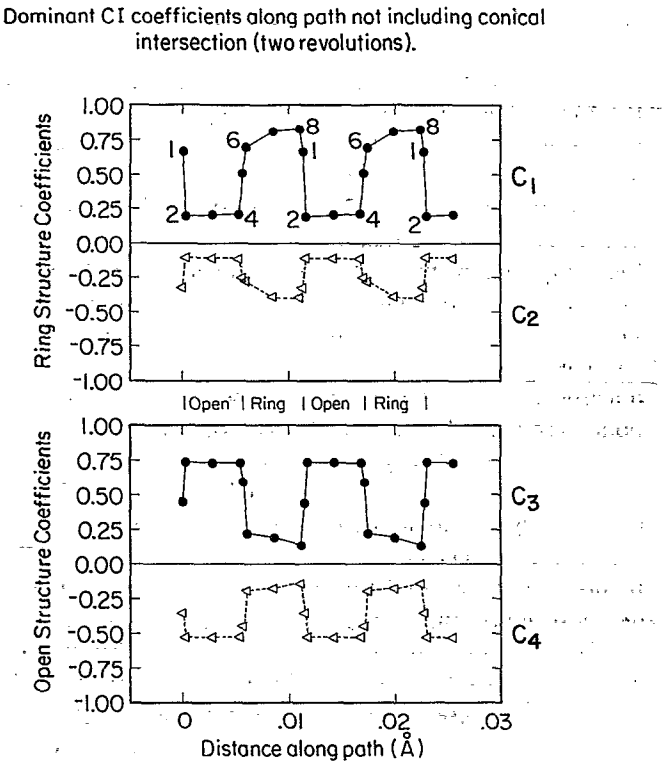

FIG. 11. Values of the CI coefficients of the four dominant configurations along the loop not including the intersection. The legend between the two panels indicates whether the points lie on the ring-structure side or the open-structure side of the barrier ridge. Two revolutions are shown.

directly related to the signs of the MC expansion coefficients of these four configurations. We shall therefore monitor these four MC expansion coefficients.

Figure 10 depicts the loops in the X–Y plane along which we shall follow the wave functions. The domain of this figure corresponds to that of the inset in Fig. 7. The shaded area in Fig. 10 indicates the location of the ridge separating the ring structure basin from the open structure basin and is thus essentially parallel to the vector **d** connecting the transition state and the intersection. The interpolated presumed intersection point is also marked. Two loops are shown: One loop encircles the intersection point, as required by the phase theorem; the other does not and serves as a "blank." On both paths, the points are indicated where the wave function is calculated: 51 points on the loop around the intersection point, 8 points around the blank loop. (It may be noted that the domain of Fig. 9 corresponds essentially to the inside of the loop encircling the intersection in Fig. 10.)

Figure 11 exhibits the variation of the coefficients of the four dominant ground-state configurations when one moves *twice* around the *blank* loop. The numbering of the points corresponds to that in Fig. 10. The abscissa of Fig. 11 is the actual distance along the loop in Fig. 10 and, hence, corresponds to the distance traveled by one of the end atoms. The legend *between* the two panels indicates the parts of the loop which are on the open-structure side (points 2,3,4) and those which are on the ring-structure side (points 6,7,8). Along both of the segments, the coefficients are seen to remain almost constant. Those on the upper panel dominate on the ring-structure side, those on the lower panel dominate on the open-structure side, as is also indicated by the ordinate labeling. Upon crossing the ridge (points 4,5,6 and points 8,1,2), the magnitudes of the coefficients change rapidly as the configurations exchange dominance. As expect-

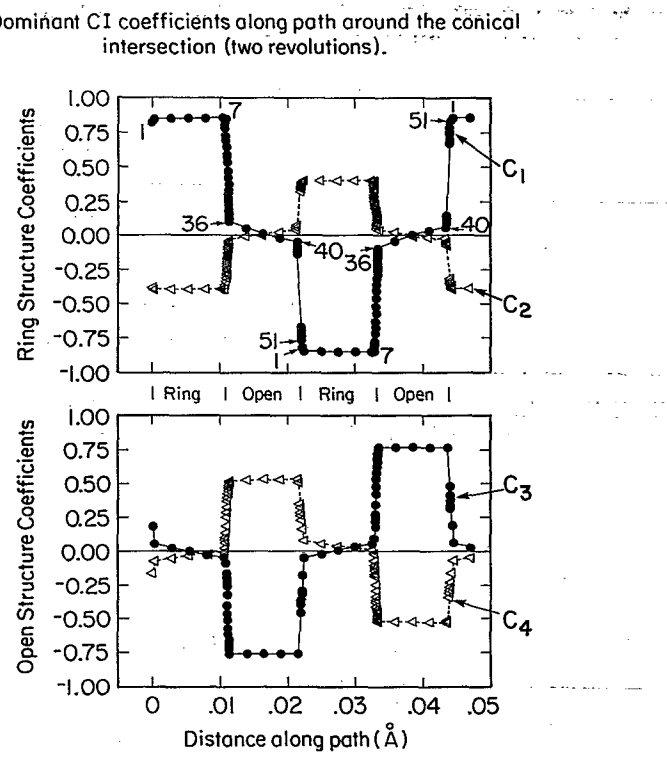

FIG. 12. Values of the CI coefficients of the four dominant configurations along the loop including the intersection. The legend between the two panels indicates whether the points lie on the ring-structure side or the open-structure side of the barrier ridge. Two revolutions are shown.

ed, all coefficients return to their original values after the loop has been traversed *once*.

Figure 12 displays the variations of the coefficients of the four dominant ground-state configurations when one travels twice around the loop *which encircles* the *intersection*. The points correspond again to those in Fig. 10. Also, in every other respect, Fig. 12 is arranged in the same manner as Fig. 11. The large number of points was chosen for the following reason. Since the calculations at various points yield wave functions with arbitrary *overall* signs, it is necessary to change these signs in such a manner that the *large* coefficients remain constant along the segments which do not cross the ridge. This is straightforward and not too many points are needed here. This forced continuity of the large terms automatically determines the signs of the small terms. However, when one crosses over the barrier, *all* coefficients change very rapidly and one must be sure with which sign each coefficient ends up on the other side of the barrier. The points must therefore be chosen rather closely in order to demonstrate continuity if our reasoning is to be conclusive.

It is seen that *all four coefficients change sign after one revolution*. Therefore, so does the wave function. It is also apparent that these coefficients account for about 80% of the normalization confirming the dominance of the corresponding configurations.

Since this entire calculation has been carried through in C_{2v} symmetry, it has been proven that an intersection *does exist in* C_{2v} *symmetry* somewhere inside the traversed loop. There can be little question that it occurs extremely close to the minimum of the quadratic determined in Table V.

C. The 1 $^1A_1$ and the 2 $^1A_1$ energy surfaces near the transition state and the intersection

It is of obvious interest to examine the shapes of the two energy surfaces in the region around the transition state and the intersection. To construct these maps, state-averaged calculations were performed at additional points. All points for which energies were eventually determined are displayed in Fig. 13. Its range in the u direction (parallel **d**) is apparent from the indicated locations of S^* and I and its range in the v direction is approximately twice as wide as the shaded region in Fig. 10. Note that the v scale is expanded by about an order of magnitude relative to the u scale. The energies at these points could be least-mean-square fitted, with an accuracy of better than 1%, by appropriate functions which were then used to map the surfaces.

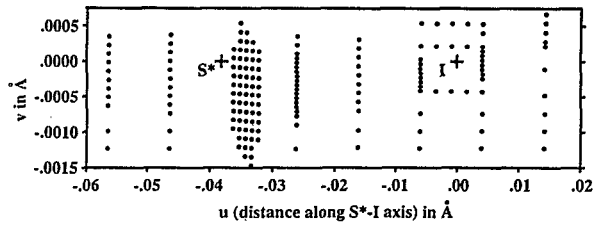

FIG. 13. Points in the neighborhood of the intersection I and the transition state S^*, where state-averaged calculations were made. Coordinates u, v defined in Sec. V B, second subsection.

In view of the first order expansion mentioned under item (ii) of Sec. V A, we chose the following higher order approximations:

$$(E_2 + E_1)/2 = E_0 + P,$$
$$(E_2 - E_1)/2 = \Delta E_0 + Q,$$

where

$$E_0 = a_1 u + a_2 v,$$
$$\Delta E_0 = \{b_1 u^2 + b_2 v^2 + b_3 uv\}^{1/2},$$
$$P,Q = \text{polynomials in } u \text{ and } v.$$

For ΔE_0, we took the earlier fit of the difference cone listed in Table V, expressed in the coordinates u and v, and divided by two. [A very small negative constant of order 10^{-13} hartree^2 was omitted under the square root so that $(E_2 - E_1)$ is real everywhere.] The coefficients a_1, a_2 were fitted together with those of the polynomial P to the average $(E_1 + E_2)/2$ and, accordingly, no linear terms were included in P. A mean absolute deviation of 0.3 microhartree, corresponding to a mean relative deviation of 0.01%, was achieved with quadratic and cubic terms and could not be improved upon by higher order terms. The coefficients of Q were fitted to the difference $[(E_2 - E_2)/2 - \Delta E_0]$. No significant improvement could be achieved by multiplying ΔE_0 with an adjustable coefficient or by having linear terms in Q. Including quadratic, cubic, and quartic terms in Q yielded a mean absolute deviation of 2.4 microhartree, corresponding to a relative mean deviation of 0.35%, which could not be improved upon by higher order terms. The resulting polynomials are listed in Table VI. Contour plots of $(E_1 + E_2)/2$ and $(E_2 - E_1)/2$ are displayed in Fig. 14. Both have a remarkably simple structure. An interesting feature is that the long axes of the curves of the two functions lie approximately at right angles to each other.

From the discussed fits, one obtains for the energies of the two states the approximations

$$E_1 = E_0 - \Delta E_0 + R_1, \quad R_1 = P - Q,$$
$$E_2 = E_0 + \Delta E_0 + R_2, \quad R_2 = P + Q.$$

For both states, the mean absolute deviation is found to be about 2.5 microhartree, corresponding to a relative mean deviation of 0.1%.

Contour plots of these approximations to E_1 and E_2 are displayed in Fig. 15. The surface for the lower state, E_1, showing the transition state as well as the intersection, has the qualitative features expected from our earlier discussion. The contours around the intersection point look somewhat different from those in Fig. 5, which were derived by a much cruder curve plotting interpolation from a very much more widely spaced grid of energy values obtained from single-state MCSCF calculations. In particular, neither the contours of E_1 nor those of E_2 look like contours of a cone near the intersection. An exhaustive discussion of possible contours near an intersection point is given in Ref. 41.

The surface for the upper state, E_2, yields a surprise. It is seen to have a *minimum* very close to the transition state of the lower surface. (Its position was also marked on Fig. 7.) We verified this feature of the fitting function by further calculations in the neighborhood of this minimum and deter-

TABLE VI. Fits to $(E_1 + E_2)/2$ and $(E_2 - E_1)/2$ for the lowest two $^1A_1$ energy surfaces in the region of their intersection.

$(E_1 + E_2)/2$	$= \bar{E}_0 + P$	ABSDV[a] = 0.3,	RELDV[b] = 0.01%
$(E_2 - E_1)/2$	$= \Delta E_0 + Q$	ABSDV = 2.4,	RELDV = 0.35%
$\bar{E}_0$	$= -224.462\,172\,0 + 0.054\,923\,u + 0.127\,92\,v$		
ΔE_0	$= \{0.000\,032\,604\,63\,u^2 - 0.002\,240\,064\,uv + 0.066\,263\,51\,v^2\}^{1/2}$		
P,Q	= polynomials in u,v with the following coefficients.		

u^iv^k	P	Q	u^iv^k	Q
u^2	0.646 374	−0.016 736	u^4	8.440 045
uv	−0.774 771	0.535 197	u^3v	−443.673 230
v^2	0.752 950	9.328 484	u^2v^2	20 906.613 471
u^3	−2.011 872	0.626 765	uv^3	−1 038 561.463 579
u^2v	2.771 779	−32.810 589	v^4	−10 019 383.305 341
uv^2	2.568 780	−1865.395 284		
v^3	40.180 176	−1060.095 301		

[a] Mean absolute deviation of E(exact) − E(fit) in microhartree.
[b] Relative absolute deviation = ABSDV ÷ [range of E(exact)] in percent.

mined its position as $\phi_x = 83.592°$, $R_x = 1.441$ Å. Next, we ascertained that the calculated energy of E_2 at the C_{2v} *symmetry breaking* point $\phi = \phi_x$, $R_1 = R_x + 0.01°$, $R_2 = R_x - 0.01°$ is 77 microhartree *higher* than that at the point ϕ_x, R_x. The latter therefore represents a minimum of the upper state in C_s symmetry. Finally, we made calculations which showed that the minimum found is the *global* minimum of this excited $^1A'$ state[42] in C_{2v} symmetry. We thus have the remarkable result that *the transition state on the* 1 $^1A_1$ surface, the *equilibrium structure on the* 2 $^1A_1$ *surface, and the intersection between both surfaces all lie within a distance of* 0.04 Å *and within* 1 *kcal/mol from each other in* C_{2v} *symmetry.*

It should be noted that, in Fig. 15, the v scale is greatly expanded with respect to the u scale. A presentation depicting u and v on the *same* scale is given in Fig. 16. The upper part of this figure displays plots of E_1 and E_2 vs u along the line connecting the transition state and the intersection point. The energy at the intersection point is seen to lie 1.2 millihartree above that of the ground-state transition state and 0.9 millihartree above that of the minimum of the dashed line which, itself, lies 0.1 millihartree above the upper state minimum (see Tables III and IV). The lower part of this figure contains plots of E_1 and E_2 vs v for various values u = constant, corresponding to seven passes across the ridge. Figure 16 clearly exhibits the considerable difference

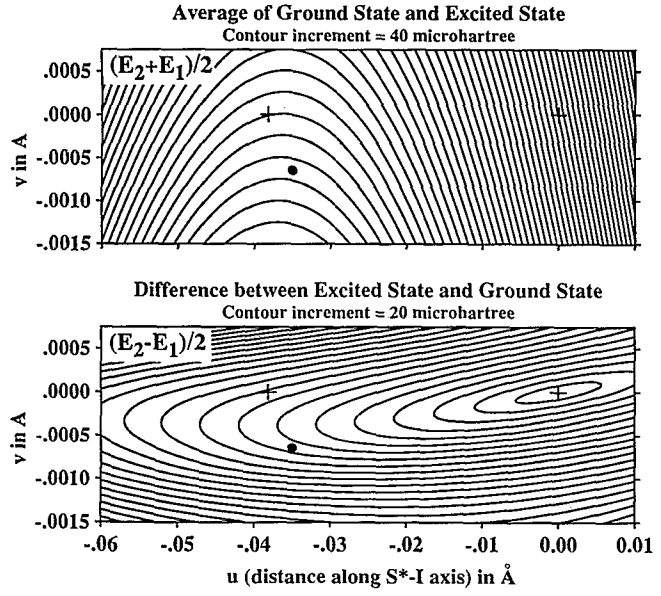

FIG. 14. Contours of the average $(E_1 + E_2)/2$ and the difference $(E_2 - E_1)/2$ in the domain around $I(u = v = 0)$ and $S^*(u = -0.038, v = 0)$, both indicated by +. $(E_1 + E_2)/2 = -224.462\,172$ hartree at I and decreasing towards negative values of u. $(E_2 - E_1)/2 = 0$ at I and increasing in all directions. The dot indicates the minimum of the upper state.

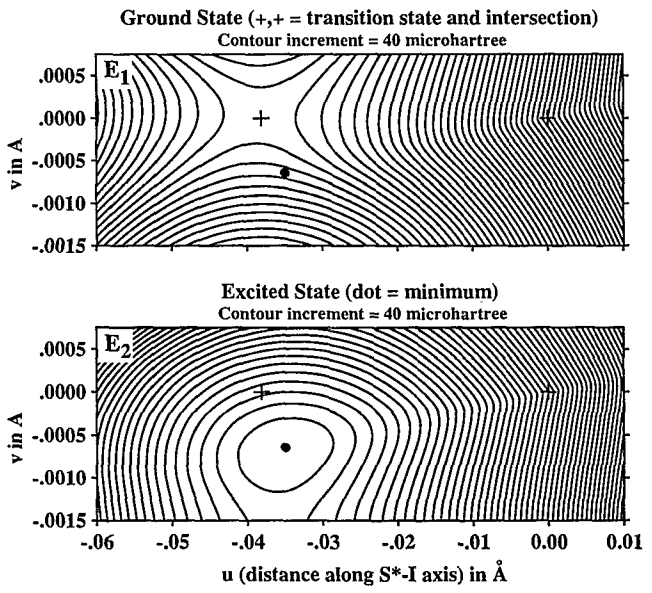

FIG. 15. Contours of the two lowest $^1A_1$ PES, E_1 and E_2, in the domain around I $(u = v = 0)$ and S^* $(u = -0.038, v = 0)$, both indicated by +. E_2 has a minimum at the point indicated by a dot. $E_1 = E_2 = -224.462\,172$ hartree at I. Both E_1 and E_2 decrease from I towards negative values of u.

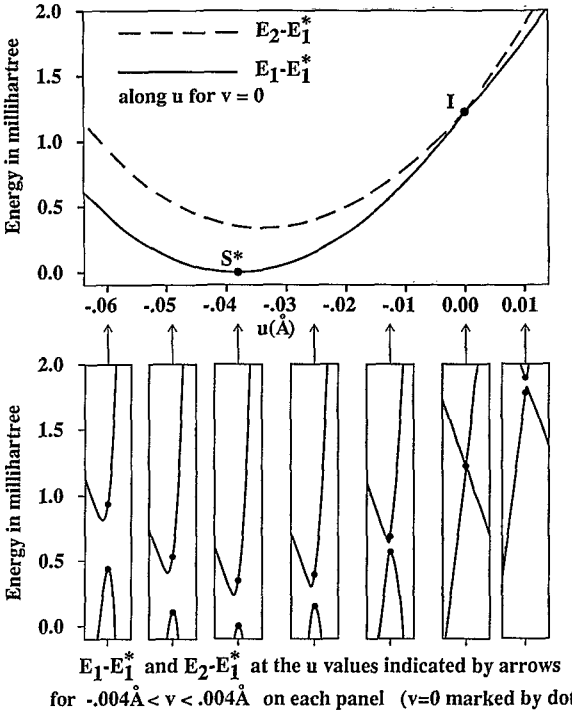

FIG. 16. The energies $(E_1 - E_1^*)$ and $(E_2 - E_1^*)$ as functions of u and v. E_1^* = transition state energy of E_1. Upper panel: energy profiles along the ridge of the barrier $(v = 0)$. Lower panels: energy profiles going across the ridge for various values of u, as indicated by arrows. The range on each lower panel goes from -0.004 Å to $+0.004$ Å.

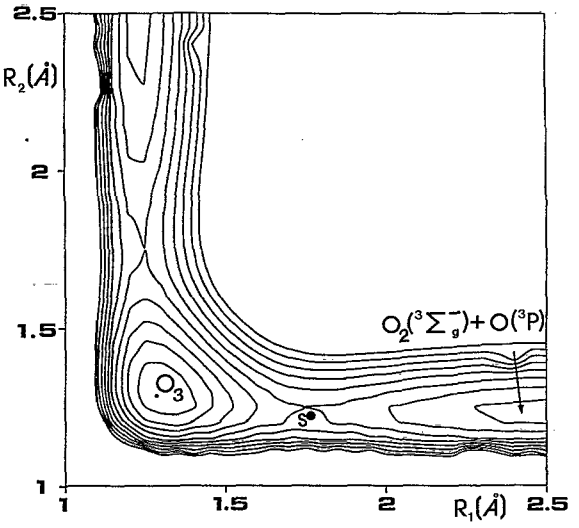

FIG. 17. Cross section through the ground-state potential energy surface of ozone for a fixed O–O–O angle of 116.31°. The ordinates R_1, R_2 are the two O–O bond lengths. Increment: 5 millihartree. The contours are based on 320 evenly spaced calculated values.

in the slopes of the energy for the directions parallel and perpendicular to the ridge for both surfaces. In the lower panels, the range of v is more than twice that considered in Figs. 13, 14, and 15. Those parts of the energy curves which fall outside the v range of Figs. 13, 14, and 15, are based on additional state-averaged MCSCF calculations.

D. The intersection seam in C_s symmetry

The dimensionality rule (i) of Sec. V A can be stated more explicitly as follows. Two energy surfaces of the same symmetry do not have to intersect. However, if they do intersect in one point, then it is to be expected (i.e., the opposite is very unlikely) that this point is part of an intersection space of dimension $(Q - 2)$. It follows then, for the case at hand, that the intersection point which we have found in C_{2v} symmetry is part of an intersection *curve* which extends into C_s symmetry. We conclude, therefore, that a one-dimensional intersection seam exists on the ground-state energy surface of ozone for nonisosceles geometries.

VI. THE DISSOCIATION $O_3 \rightarrow O_2 + O$

From Fig. 1 it is apparent that abstraction of the central atom to form $O + O_2$ under preservation of C_{2v} symmetry is a quite unrealistic dissociation channel since it has a composite barrier of about 77 kcal/mol. More likely candidates for this important reaction are C_{2v} symmetry-breaking dissociation channels where one end atom flies off, leaving the other behind to form O_2. Calculations of such dissociations involve greater geometric variability and larger number of configurations (8029) than the C_{2v} restricted calculations of the earlier sections.

In the absence of any other information, we chose to examine the reaction

$$O_3(^1A_1) \rightarrow O_2(^3\Sigma_g^-) + O(^3P),$$

with the O–O–O angle fixed at 116.31°, the apex angle of the open structure ground-state minimum. We calculated ground-state energies for ϕ fixed at this angle and 160 values of R_1, R_2 (the bond lengths from the central atom to the end atoms) with $R_1 \leqslant R_2$. This yielded 320 fairly evenly spaced energy values for generating the contour plot displayed in Fig. 17, which furnishes the cross section through the full potential energy surface for $\Phi = 116.31°$. The contour increment is 5 millihartree. The potential rises smoothly from a shallow well at the open-structure minimum to an atom–plus–diatom channel along the valley corresponding to the $O_2 + O$ dissociation. A feature not found in an analogous plot by Wilson and Hopper[21] is a saddle point in this dissociation channel at $\phi = 116.31°$, with $R_1 = 1.233$ Å, $R_2 = 1.759$ Å with the energy $E = -224.528\,261$ hartree. It implies a barrier of 15.1 kcal/mol for the dissociation process when ϕ is kept fixed at 116.31°. Dissociation along a C_s path is therefore favored over abstraction along the C_{2v} path with a 77 kcal/mol barrier.

Starting from this saddle point, we located the true transition state of the dissociation along the minimum energy path on the $^1A'$ surface in C_s symmetry. While the gradient at the saddle point of the $\phi = 116.31°$ panel has zero components with regard to the R_1 and R_2 internal coordinates, it has a nonzero component with regard to the bending angle ϕ, indicating that it is not a stationary point on the full ground-state PES. However, this nonzero component of the gradient is quite small and the Hessian has only one negative eigenvalue corresponding to a normal mode. These data, taken together, suggest that we are close to a transition state which lies more or less in the direction of a change in the ring open-

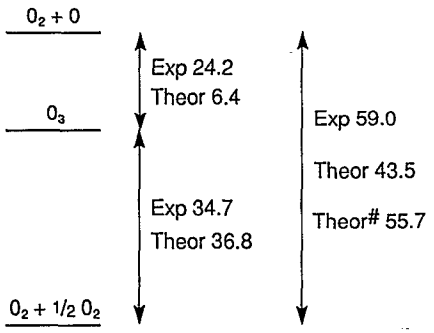

FIG. 18. Reaction energies (including changes in vibrational zero-point energies) in kcal/mol for the systems, O_3, $O_2 + O$, $O_2 + \frac{1}{2}O_2$. Exp = experimental values (see Sec. I A). Theor = theoretical values from FORS calculations. Theor# = theoretical values from FORS calculation of O_2 including intra-atomic-correlation-correction (Ref. 43).

ing angle ϕ. A transition state search going uphill in this direction was initiated at S^* and lead to a structure with the coordinates $\phi = 114.90°$, $R_1 = 1.234$ Å, $R_2 = 1.759$ Å. At this point, the gradient was zero and the Hessian was found to have two positive eigenvalues and one negative eigenvalue (with frequencies 63.3, 422.5, and 96.3i cm^{-1}, respectively). This point is therefore the transition state on the full ground-state $^1A'$ surface for the dissociation process along a C_s path. Including the harmonic zero point energies at the open minimum (4.0 kcal/mol) and at the dissociation transition state (0.7 kcal/mol), the barrier for this dissociation is calculated to be 11.7 kcal/mol.

The dissociation energy is calculated to be 8.5 kcal/mol, which is substantially lower than the experimental value (26.0 kcal/mol, see Sec. I A). A very similar error of the full valence MCSCF approach had been found some time ago[43] for the dissociation of O_2 into 2O. The relevant quantities, including the changes in vibrational zero-point energies (see Sec. I A), are summarized in Fig. 18. While the exothermicity of the reaction $O_3 \rightarrow (3/2)\ O_2$ is seen to be predicted quite well, the dissociation energies for $\frac{1}{2}\ O_2 \rightarrow O$ and $O_3 \rightarrow O_2 + O$ have errors of 14.4 kcal/mol and 15.7 kcal/mol, respectively. Only about 10% of them can be removed by improvements in the basis sets.[44] It must therefore be concluded that dynamic correlation is considerably weaker in the oxygen atom than in the molecules O_3 and O_2. The difficulty of obtaining good values for these dissociation energies from pure *ab initio* calculations has recently been documented by the extensive work [including MBP and coupled cluster (CC) calculations] of Rama Krishna and Jordan.[44] However, in O_2, the missing dynamic correlation change can be recovered rather effectively by the intra-atomic-correlation-correction of the molecular FORS wave function, as we have shown in Ref. 43. It is therefore likely that the inclusion of this correction in our ozone wave function will also reduce the error in the $O_3 \rightarrow O_2 + O$ dissociation to a few kcal/mol. The experimental dissociation energy of O_2 can be recovered within 0.3 kcal/mol by a calculation in which the FORS wave function is augmented by all single and double excitations in a $3s2p2d\,2f\,1g$ basis.[45] The same success can therefore be expected for the dissociation of O_3.

In view of these results, it is likely that the energy lowering from the saddlepoint on Fig. 17 to the dissociated products is a consequence of the progressively increasing improvement in the quality of the wave function with increasing R_1 values. If this assessment is correct, then the energy for a wave function of consistent quality will increase without barrier to the experimental dissociation energy value as R_1 increases. Nonetheless, the calculated transition state may very well indicate the energetically most favorable angle ϕ for dissociation.

In any event, there are good reasons to be confident that such a long-range variability of the wave function quality has no implication for the short distances covered in the energy difference Table IV. This inference is confirmed by the agreement with the earlier mentioned calculations of Lee at the two minima[24] and by the fact that the FORS-type wave function yields the correct energy change for the dissociation $2O_3 \rightarrow 3O_2$ (see Fig. 18). The relative energy changes displayed in the earlier figures therefore provide a credible basis for the conclusions reached in the preceding sections.

VII. SUMMARY

In the present investigation, potential energy surface cross sections are determined which pertain to two aspects of the ozone ground state: the relation between the two equilibrium structures and the dissociation into $O_2 + O$. In order to deal with the considerable configurational changes that occur across such surfaces, the full valence space MCSCF approach (FORS) was chosen and a double-zeta-plus-polarization type basis set was used.

Light was shed on the unresolved aspects of the first problem. The potential energy surface encompassing the ring and the open minimum, as well as the reaction path between them, was determined and the ring opening transition state was found. The latter was shown to have C_{2v} symmetry and to lie almost as high above the ring minimum (22.7 kcal/mol) as the open minimum lies below it (30.2 kcal/mol). The ring structure lies somewhat above the experimental ($O_2 + O$) dissociation limit. It is apparent that these energetics make it difficult to access the ring directly.

Very close to the transition state, an interesting feature was discovered: A conical intersection between the ground state and an excited state of the same symmetry ($^1A_1$ in C_{2v}, $^1A'$ in C_s). Its existence in C_{2v} symmetry was conclusively proven by application of the phase change theorem and the difference cone was mapped out. This result implies the extension of an intersection seam between the two states into C_s symmetry. This is the first accurate *ab initio* example of such an intersection for a bound ground state and, also, for a molecule in C_{2v} symmetry. In addition, the excited state surface was found to have its minimum very close to the transition state geometry of the ground-state surface. The two energy surfaces are depicted by the perspective drawing of Fig. 19 which covers the same range as Figs. 14, 15, and 16. These remarkable potential energy surface features can have considerable implications regarding the radiationless activation and deactivation of ozone. However, more information about the excited $^1A'$ state is needed to justify detailed inferences. We are currently examining the energy surface of this state over a more extended range.

The results regarding the dissociation of ozone into

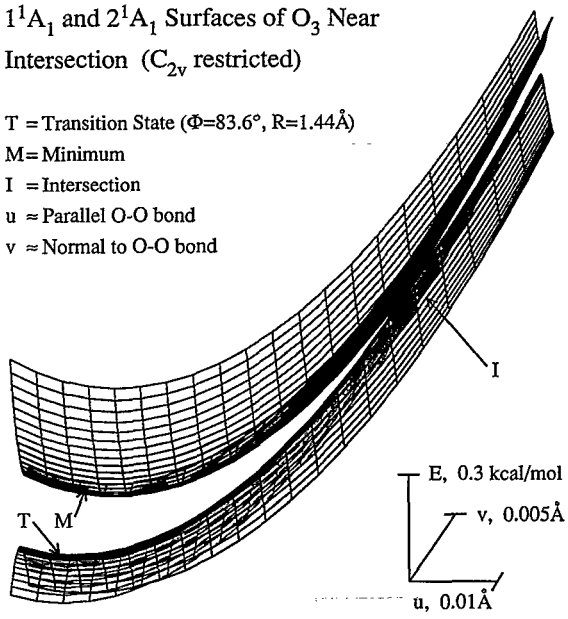

FIG. 19. Perspective representation of the $1\ ^1A_1$ and the $2\ ^1A_1$ energy surfaces of ozone over the coordinate range covered in Figs. 14, 15, and 16.

$O_2 + O$ show that the ring minimum connects with the $(O_2 + O)$ ground state through abstraction of the central atom. Easier is, however, the detachment of an end atom from the open minimum via a path through C_s symmetry. The results obtained suggest that the energetically most favorable angle for dissociation is not too different from the apex angle in the open-minimum structure.

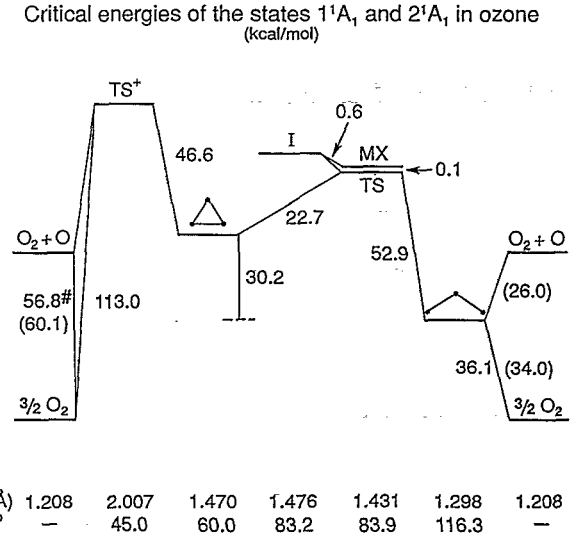

FIG. 20. Energy differences of PES' of three oxygen atoms (in kcal/mol) exclusive of zero-point vibration energies. TS: transition state between ground-state ring and open structure. TS^+: ground-state transition state for abstraction of the central oxygen. I: intersection between the ground state and the lowest excited state of like symmetry. MX: minimum of the latter. R,ϕ = bond length and apex angle in C_{2v} symmetry. Numbers without parentheses calculated in the present work. # indicates calculation with FORS intra-atomic-correlation-correction method. Parentheses denote experimental values adjusted for changes in zero-point vibrational energies (see Sec. I A). Distances between levels are drawn to scale except for the separations between TS, MX, and I which are exaggerated.

The various discussed energy differences obtained by the present work were summarized in Tables III and IV and are graphically displayed in Fig. 20. Because of the problem with the O_2 dissociation discussed in the preceding section, the intra-atomic-correlation-corrected value is shown for it. The numbers displayed do *not* include the changes in the vibrational zero-point energy. The quoted experimental values are adjusted accordingly by the zero-point energies as discussed in Sec. I A.

ACKNOWLEDGMENTS

The Ames Laboratory is operated for the U.S. Department of Energy by Iowa State University under Contract No. W-7405-Eng-82. This work was supported by the Division of Chemical Sciences, Office of Basic Energy Sciences. A grant for computer time on the CRAY–YMP computer by the Pittsburgh Supercomputer Center of the National Science Foundation is also acknowledged.

[1] G. Herzberg, in *Molecular Spectra and Molecular Structure: III. Electronic Structure of Polyatomic Molecules* (Van Nostrand, New York, 1966).
[2] *JANAF Thermochemical Tables*, J. Phys. Chem. Ref. Data (Am. Chem. Soc. and Am. Inst. Phys. for U.S. Nat. Bur. Standards), Vol. 14, Suppl. 1 (1985).
[3] K. P. Huber and G. Herzberg, in *Molecular Spectra and Molecular Structure: IV. Constants of Diatomic Molecules* (Van Nostrand, New York, 1979).
[4] *Ionization Potential and Appearance Potential Measurements 1971-1981*, edited by Rhoda D. Levin and Sharon G. Lias (U.S. Nat. Bur. Stand., 1982).
[5] *Gas-Phase Ion and Neutral Thermochemistry*, J. Phys. Chem. Ref. Data (Am. Chem. Soc. and Am. Inst. Phys. for U.S. Nat. Bur. Standards) Vol. 17, Suppl. 1 (1988).
[6] C. J. Hochanadel, J. A. Ghormley, and J. W. Boyle, J. Chem. Phys. **48**, 2416 (1968).
[7] J. F. Riley and R. W. Cahill, J. Chem. Phys. **52**, 3297 (1970).
[8] P. L. T. Bevan and G. R. A. Johnson, J. Chem. Soc. Faraday Trans. I **69**, 216 (1973).
[9] C. W. von Rosenberg, Jr., and D. W. Trainor, J. Chem. Phys. **61**, 2442 (1974).
[10] P. G. Burton and M. D. Harvey, Nature **226**, 826 (1977).
[11] J. S. Wright, Can. J. Chem. **51**, 139 (1973).
[12] P. J. Hay and W. A. Goddard III, Chem. Phys. Lett. **14**, 46 (1972).
[13] P. J. Hay, T. H. Dunning, Jr., and W. A. Goddard III, Chem. Phys. Lett. **23**, 457 (1973).
[14] S. Shih, R. J. Buenker, and S. D. Peyerimhoff, Chem. Phys. Lett. **28**, 463 (1974).
[15] P. J. Hay, T. H. Dunning, Jr., and W. A. Goddard III, J. Chem. Phys. **62**, 3912 (1975).
[16] L. B. Harding and W. A. Goddard III, J. Chem. Phys. **67**, 2377 (1977).
[17] R. R. Lucchese and H. F. Schaefer III, J. Chem. Phys. **67**, 848 (1977).
[18] T. H. Dunning and P. J. Hay, J. Chem. Phys. **67**, 2290, (1977).
[19] G. Karlström, S. Engström, and B. Jönsson, Chem. Phys. Lett. **57**, 390 (1978).
[20] P. G. Burton, J. Chem. Phys. **71**, 961 (1979).
[21] C. W. Wilson, Jr., and D. G. Hopper, J. Chem. Phys. **74**, 595 (1981).
[22] R. O. Jones, J. Chem. Phys. **82**, 325 (1985).
[23] F. Moscardo, R. Andarias, and E. San-Fabian, Int. J. Quantum Chem. **34**, 375 (1988).
[24] T. J. Lee, J. Chem. Phys. **93**, 489 (1990); Chem. Phys. Lett. **169**, 529 (1990).
[25] J. N. Murrell, S. Carter, S. C. Farantos, P. Huxley, and A. J. C. Varandas *Molecular Potential Energy Functions* (Wiley, New York 1984), Sec. 10.1.
[26] S. Xantheas, S. T. Elbert, and K. Ruedenberg, J. Chem. Phys. **93**, 7519 (1990).
[27] P. E. H. Siegbahn, A. Heiberg, B. O. Roos, and B. Levy, Phys. Scr. **21**, 323 (1980); B. O. Roos, P. R. Taylor, and P. E. M. Siegbahn, Chem. Phys. **48**, 157 (1980).

[28] K. R. Sundberg and K. Ruedenberg, *Quantum Science*, edited by J. L. Calais, O. Goscinski, J. Linderberg, and Y. Öhrn (Plenum, New York, 1976) p. 505ff; M. Gilbert-Dombek, Ph.D. thesis, Iowa State University, 1977; K. Ruedenberg, Proceedings of the August 1978 NRCC Workshop on post-Hartree–Fock Quantum Chemistry and Configuration Interaction (Lawrence Berkeley Laboratory, University of California, 1979), p. 46; L. M. Cheung, K. R. Sundberg, and K. Ruedenberg, Int. J. Quantum Chem. **16**, 1103 (1979).
[29] T. H. Dunning and P. J. Hay, in *Methods of Electronic Structure Theory*, edited by H. F. Schaefer (Plenum, New York, 1977), Vol. III, p. 1.
[30] M. Dupuis, D. Spangler, and J. J. Wendoloski, Nat. Resour. Comput. Chem. Software Cat 1, Prog. QG01 (GAMESS) (1980).
[31] H.-J. Werner and P. J. Knowles, J. Chem. Phys. **82**, 5053 (1985); Chem. Phys. Lett. **115**, 259 (1985).
[32] A. J. C. Varandas, J. Tennyson, and J. N. Murrell, Chem. Phys. Lett. **61**, 431 (1979).
[33] J. Katriel and E. R. Davidson, Chem. Phys. Lett. **76**, 259 (1980).
[34] M. R. Manaa and D. R. Yarkony, J. Chem. Phys. **93**, 4473 (1990).
[35] F. Hund, Z. Physik **40**, 742 (1927); J. von Neumann and E. Wigner, Physik Z. **30**, 467 (1929).
[36] E. Teller, J. Phys. Chem. **41**, 109 (1937).
[37] G. Herzberg and H. C. Longuet-Higgins, Disc. Faraday Soc. **35**, 77 (1963).
[38] H. C. Longuet-Higgins, Proc. R. Soc. London **A344**, 147 (1975).
[39] C. A. Mead, J. Chem. Phys. **70**, 2276 (1979).
[40] C. A. Mead and D. G. Truhlar, J. Chem. Phys. **70**, 2284 (1979).
[41] G. Atchity, S. Xantheas, and K. Ruedenberg, J. Chem. Phys. (in press).
[42] S. T. Elbert and K. Ruedenberg (unpublished).
[43] M. W. Schmidt, M. T. B. Lam, S. T. Elbert, and K. Ruedenberg, Theor. Chim. Acta **68**, 69 (1985).
[44] M. V. Rama Krishna and K. D. Jordan, Chem. Phys. **115**, 423 (1987).
[45] G. Atchity, S. T. Elbert, and K. Ruedenberg (unpublished).